THREE-DIMENSIONAL VIBRATION ISOLATOR FOR SUPPRESSING HIGH-FREQUENCY RESPONSES FOR SAGE III CONTAMINATION MONITORING PACKAGE (CMP)

Y. Li, S. Cutright, R. Dyke, J. Templeton, J. Gasbarre, F. Novak
NASA Langley Research Center, Hampton, VA, 23681, USA

The Stratospheric Aerosol and Gas Experiment (SAGE) III - International Space Station (ISS) instrument will be used to study ozone, providing global, long-term measurements of key components of the Earth's atmosphere for the continued health of Earth and its inhabitants. SAGE III is launched into orbit in an inverted configuration on SpaceX's Falcon 9 launch vehicle. As one of its four supporting elements, a Contamination Monitoring Package (CMP) mounted to the top panel of the Interface Adapter Module (IAM) box experiences high-frequency response due to structural coupling between the two structures during the SpaceX launch. These vibrations, which were initially observed in the IAM Engineering Development Unit (EDU) test and later verified through finite element analysis (FEA) for the SpaceX launch loads, may damage the internal electronic cards and the Thermoelectric Quartz Crystal Microbalance (TQCM) sensors mounted on the CMP. Three-dimensional (3D) vibration isolators were required to be inserted between the CMP and IAM interface in order to attenuate the high frequency vibrations without resulting in any major changes to the existing system. Wire rope isolators were proposed as the isolation system between the CMP and IAM due to the low impact to design. Most 3D isolation systems are designed for compression and roll, therefore little dynamic data was available for using wire rope isolators in an inverted or tension configuration. From the isolator FEA and test results, it is shown that by using the 3D wire rope isolators, the CMP high-frequency responses have been suppressed by several orders of magnitude over a wide excitation frequency range. Consequently, the TQCM sensor responses are well below their qualification environments. It is indicated that these high-frequency responses due to the typical instrument structural coupling can be significantly suppressed by a vibration passive control using the 3D vibration isolator. Thermal and contamination issues were also examined during the isolator selection period for meeting the SAGE III-ISS instrument requirements.

KEYWORDS: structural analysis, high-frequency response, three-dimensional vibration isolator

1. Introduction

The first SAGE instrument was launched about thirty-six years ago and SAGE III on ISS is the fourth generation of a series of NASA Earth-observing instruments. The most developed, SAGE III will be mounted on the ISS to make long-term measurements of ozone, aerosols, water vapour, and other gases in Earth's atmosphere (see Figure 1). The SAGE III on ISS mainly consists of the Interface Adapter Module (IAM), the Contamination Monitoring Packages (CMPs), the Hexapod Electronics Unit (HEU), the ExPRESS Payload Adapter (ExPA), the Instrument Control Electronics (ICE), the Sensor Assembly (SA), the Hexapod Mechanical Assembly (HMA), and the Disturbance Monitoring Package (DMP), as shown in Figure 2. The CMP #1 position (at the top panel of the IAM due to project design requirements) causes structural coupling that leads to high-frequency responses when subjected to the SpaceX launch loads. The typical structural coupling happens whenever a relatively rigid structure such as the CMP is mounted on a flexible surface such as the IAM top panel with rigid connection using mounting bolts. In order to totally suppress the high-frequency responses without any major changes to the existing CMP and IAM design, 3D vibration isolators were required to be inserted between the CMP and IAM interface, decoupling the structural stiffness over the high frequency range.

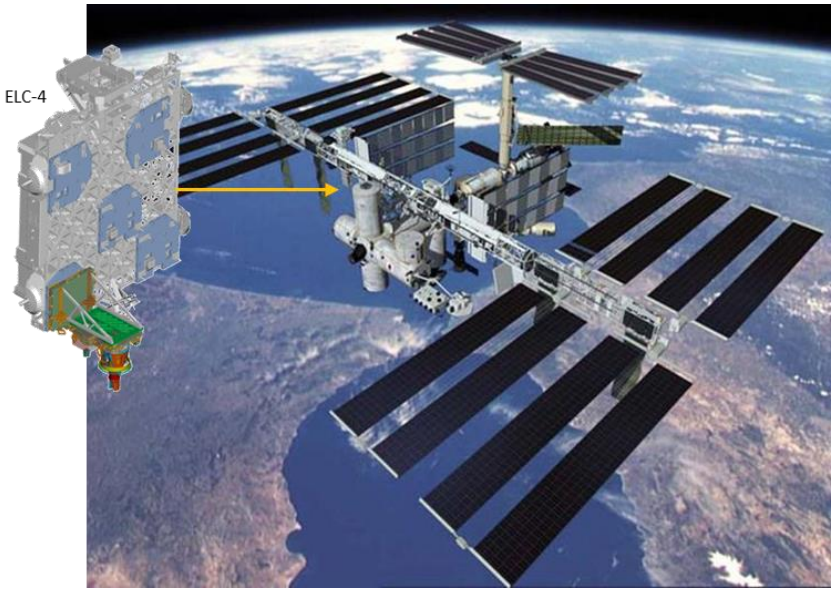

Figure 1: SAGE III on ISS

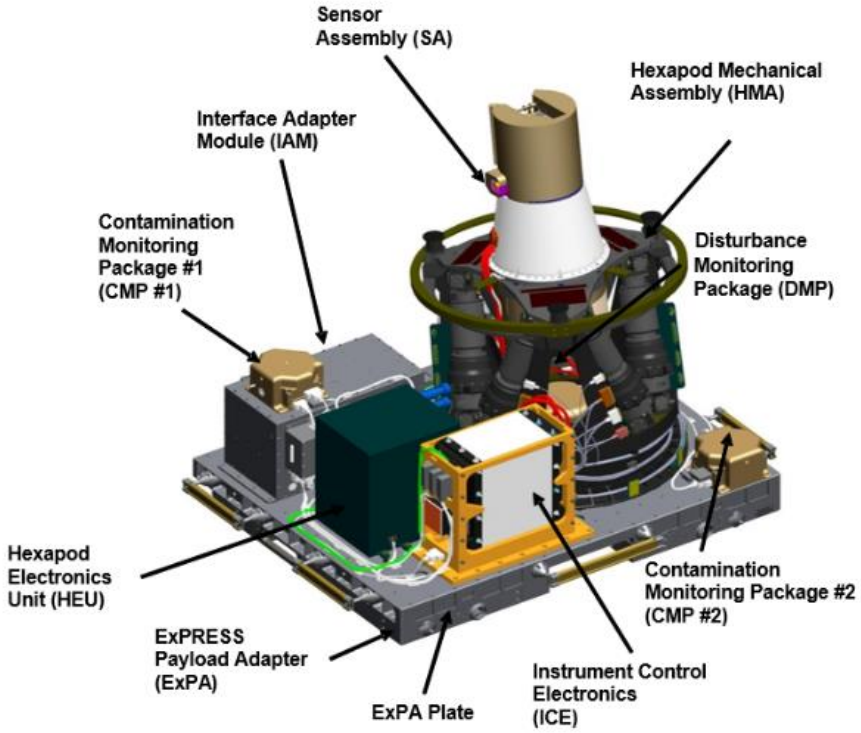

Figure 2. SAGE III on ISS Configuration

Numerous isolation systems have been developed for suppressing vibrations (Refs. 1-9). A full spacecraft vibration isolator for the James Webb Space Telescope was described utilizing four passively damped beams connecting the corners of the spacecraft to a thermal isolation tower positioning the telescope (Ref. 1). A developed analysis approach based upon a fractional derivative model of the viscoelastic material employed modal data from a finite element model. A six-axis vibration isolation, suppression and steering system was investigated and simulation was conducted in SIMULINK/MATLAB (Ref. 2). An isolator with an articulated chain of six rolamite joints arranged to give the spacecraft and subsystems full relative mobility was presented (Ref. 3). This mobility decoupled spacecraft and subsystem motions, enabling agile missions where the system bus and subsystems slew independently. Several damping and isolation approaches were discussed, including viscoelastic constrained-layer damping and magnetic tuned-mass damping of a mirror segment, passive isolation of spacecraft disturbances, and active optical telescope pointing control (Ref. 5). A method for predicting the performance of multiple mount passive isolation systems was presented (Ref. 7). Isolator design guidelines were developed for the single and multiple isolator mounting

systems. Through the years, isolation systems with the aforementioned effective vibration suppressing functions have been investigated and studied with development of isolator design and increased numerical analysis capability.

Compact wire rope isolators (WRIs) were proposed to be the 3D isolation system providing the following benefits:

- Multi-axis isolation (total 3D vibration suppression)
- Small amount of mass added to the system (about 1 lbs with four WRIs used here)
- Made of stainless steel and aluminium (no contamination issue)
- Operation temperature range: -150ºF to 500ºF (-100ºC to 260ºC) (no thermal issue for the isolator structure itself)
- No additional design requirement for installation

This paper presents the IAM FE models with different detailed configurations, the CMP FE model, and discussions on their application scopes in Section 2. Along with test data, high-frequency responses from structural analysis using the IAM and CMP FE models are presented in Section 3 where the IAM and CMP FE models are verified by comparing modal analysis results to test data. WRIs are introduced and a FE model that incorporates four WRIs into the system is described in Section 4. Random analysis results are presented in Section 5 demonstrating efficiency of the 3D isolators in suppressing the high-frequency responses, meanwhile test setups are described and test data are shown for verification. The paper ends with concluding remarks in Section 6.

2. Structural Analysis Models

The FE model 1 for the IAM, shown in Figure 3, was constructed using shell elements and different colours represent different thickness of the IAM panels. The CMP, the PDU assembly, the 120 volt contingency assembly, the computer cards assembly, and the doghouse (an interface box mounted on the IAM rear panel) were modelled as lumped masses. Since the model is representative of the IAM overall structure stiffness, it was used for modal analysis, random analysis, and kick loads analysis (induced by extravehicular activity by an astronaut). In general the FE shell model 1 is used for dynamic analysis along with limited stress analysis at some local areas because it lacks structure detailed configuration by using shell elements.

The FE model 2 for the IAM, shown in Figure 4, was constructed using solid elements. The bolts and pins that connect the chassis panels, as well as the internal bolt standoffs, were modelled as beam elements. Rigid elements were used to connect the bolts/standoffs to the chassis/cards/internal components. In addition, the PDU assembly and 120 volt contingency assembly were modelled as detailed configurations. Since the model is representative of the IAM detailed structure configuration, it was used for static g-load stress analysis, thermal stress analysis, and modal analysis regarding the internal components. In general the FE solid model 2 is used for stress analysis along with limited dynamic analysis because of its large model size.

The FE model for the CMP shown in Figure 5 was constructed using solid elements for the chassis, while the card/heat sink assembly was represented as shell elements. The bolts that connect the card/heat sink assembly were modelled as beam elements. The bolt standoffs were modelled as beam elements. Rigid elements were used to connect the bolts/standoffs to the chassis/cards/heat sink. The detailed model is used for all CMP analyses that are required by SAGE III.

For a combined FE model of the IAM and CMP that describes the CMP mounted on the top panel of the IAM configuration, the differential equations of motion for them can be written as:

$$\begin{bmatrix} M_{IAM} & 0 \\ 0 & M_{CMP} \end{bmatrix} \begin{Bmatrix} \ddot{u}_{IAM} \\ \ddot{u}_{CMP} \end{Bmatrix} + \begin{bmatrix} C_{IAM} & 0 \\ 0 & C_{CMP} \end{bmatrix} \begin{Bmatrix} \dot{u}_{IAM} \\ \dot{u}_{CMP} \end{Bmatrix} + \begin{bmatrix} K_{IAM} & K_{coupled} \\ K_{coupled}^{T} & K_{CMP} \end{bmatrix} \begin{Bmatrix} u_{IAM} \\ u_{CMP} \end{Bmatrix} = \begin{Bmatrix} E_{IAM} \\ 0 \end{Bmatrix} \quad (1)$$

where M is the mass matrix, C is the damping matrix, K is the stiffness matrix, and E is the excitation vector. It is seen from the equation (1) that even though the excitation is applied only on the IAM, the CMP vibrates with high–frequency responses due to the stiffness coupling $K_{coupled}$. The typical coupling is caused by installing the CMP on the top panel of the IAM. The IAM partition structure design and the stiff chassis give rise to the high-frequency responses of the CMP when the IAM interface is subjected to the SpaceX launch random excitations.

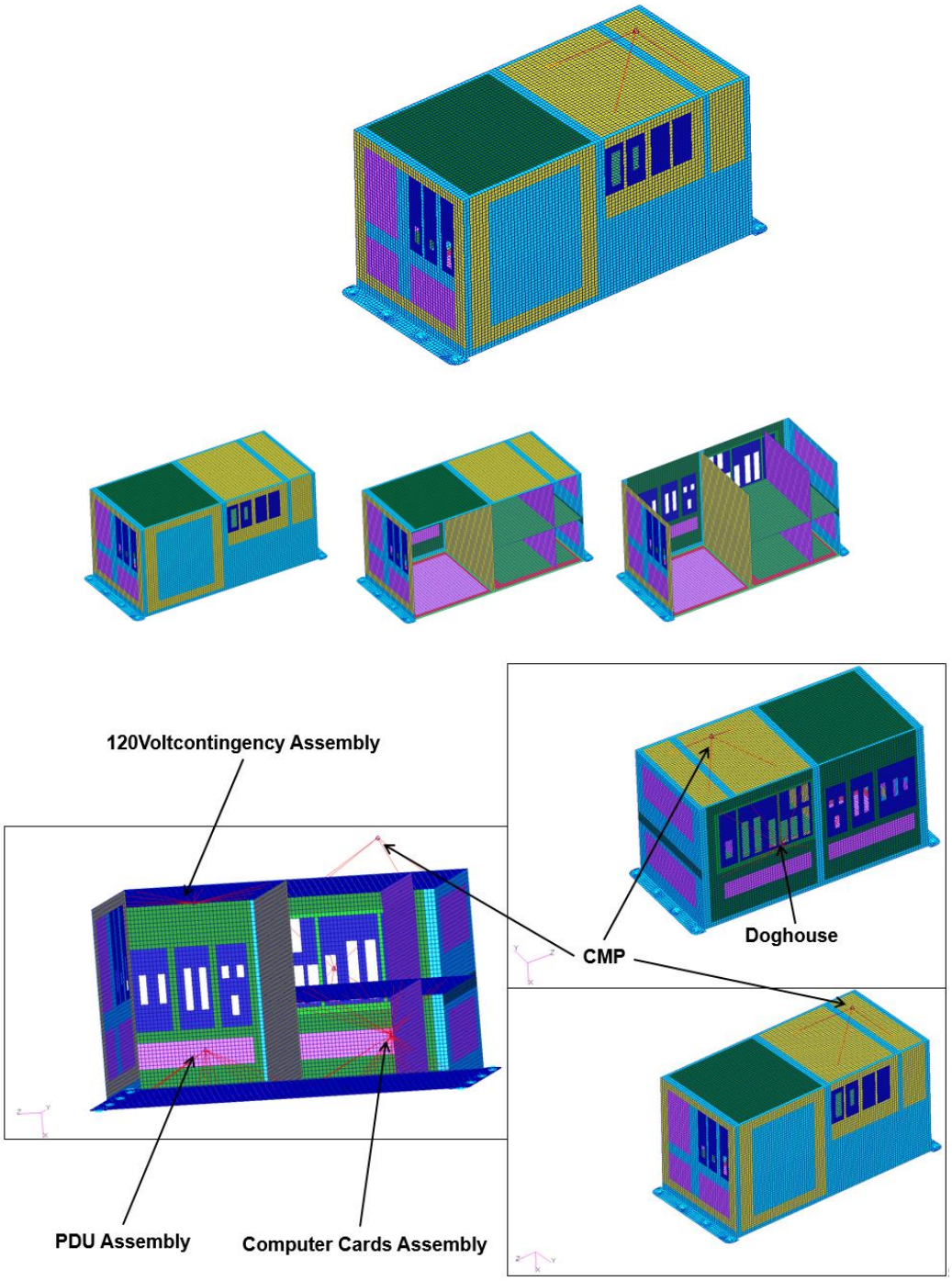

Figure 3. IAM FE Model 1

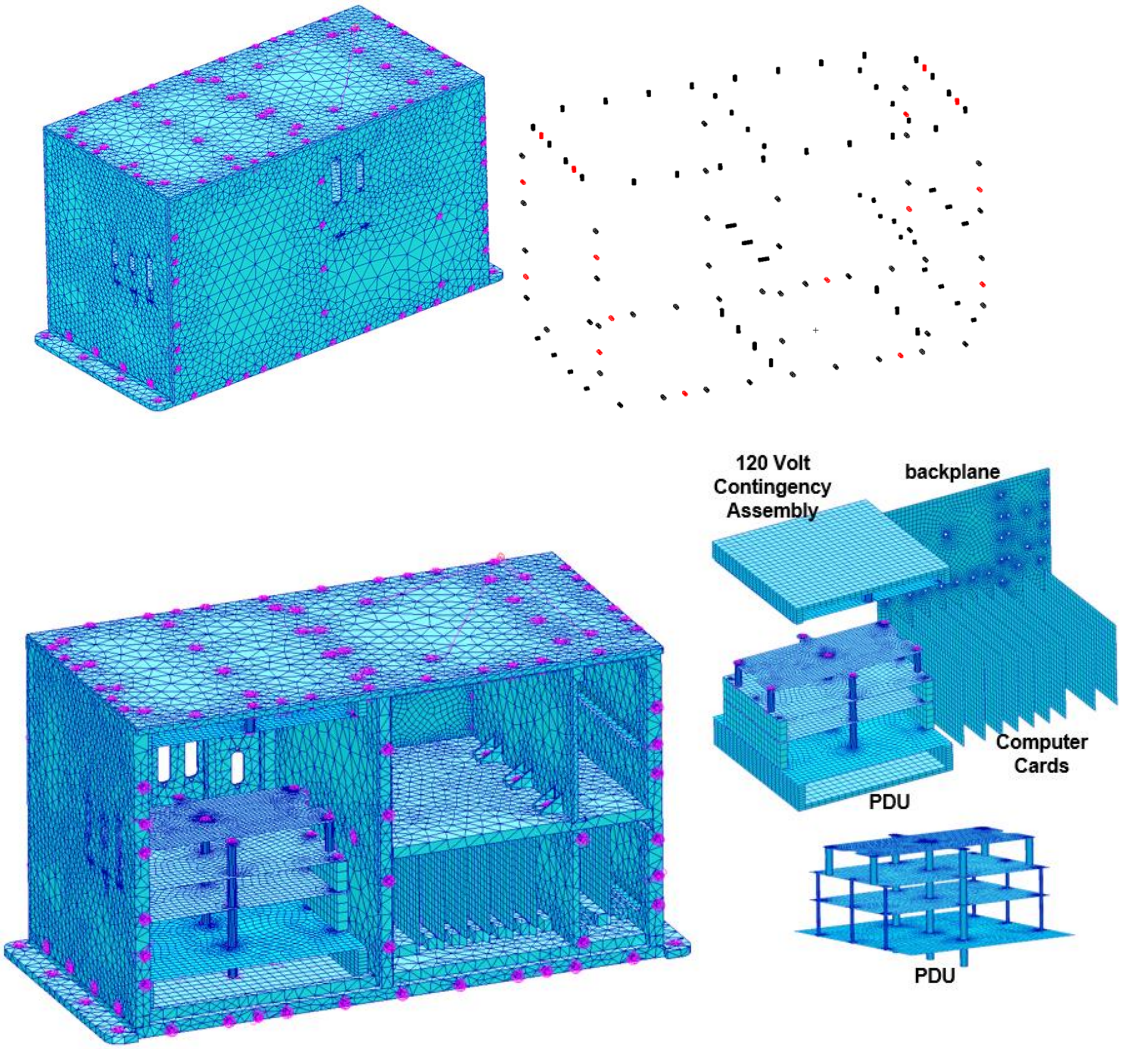

Figure 4. IAM FE Model 2 [chassis bolts (102) in black and pins (16) in red]

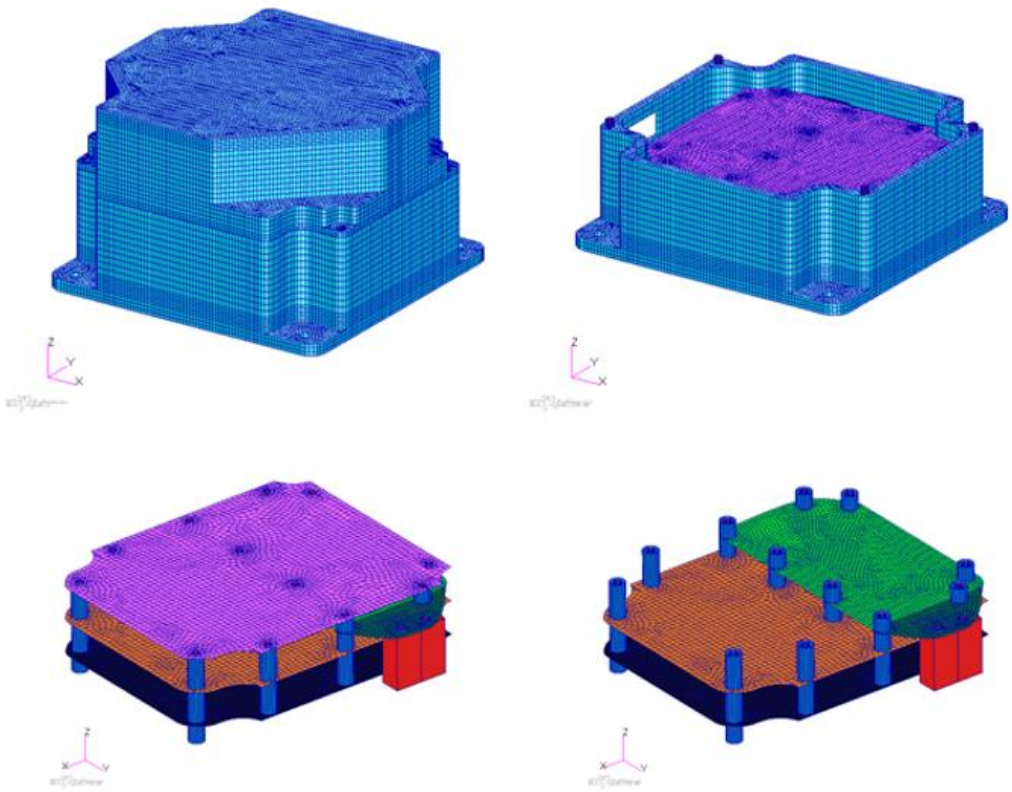

Figure 5: CMP FE Model

3. Modal Analysis and High-Frequency Responses

Modal analyses were conducted by using the aforementioned FE models and the results are correlated well with test data. The first natural frequency of the IAM and CMP system is found at about 141 Hz in modal analysis and 140 Hz in test data. As shown in Figure 6, this first mode is a PDU bouncing mode on the IAM chassis. A PDU lateral mode with 260 Hz found in analysis shows good agreement with the peak response obtained in test data shown in Figure 6. In Figure 7, the first mode associated with the CMP is the CMP lateral mode at 229 Hz found in a modal analysis and about 200 Hz obtained in test. The show good agreement considering that the IAM chassis is bolted structure and the analysis model for the result is a stitched shell structure.

Random vibration loads provided by SpaceX were input to the base of the ExPA. IAM interface responses were recovered to develop the analysis and test input levels that are the most critical loads for analysis and test. With the SpaceX launch loads, it was found from analysis

shown in Figure 8 that the CMP at the TQCM sensor locations experience high-frequency responses. These are higher than that of the TQCM sensor qualification environment indicating that the CMP high-frequency responses may cause damage to the TQCM sensors mounted on the CMP. Five sensor locations were investigated showing similar response pattern with large responses between 700 Hz and 2000 Hz. It was also found in analysis and test as well that the random load in one direction can result in high-frequency response in another direction. For instance, as shown in Figure 9, test data at the test accelerometer location R3 in the y direction demonstrates high-frequency response due to the IAM interface random load in the z direction. In order to suppress the high-frequency responses in all directions, three-dimensional (3D) isolators were required to be inserted at the interface between the IAM and the CMP. Providing 3D stiffness capacity without complicated nonlinear behaviour, isolators were also expected to be light-weight with low impact to the existing system, low contamination, and low cost. After investigation, WRIs were selected to meet all these requirements without causing major changes to the existing system.

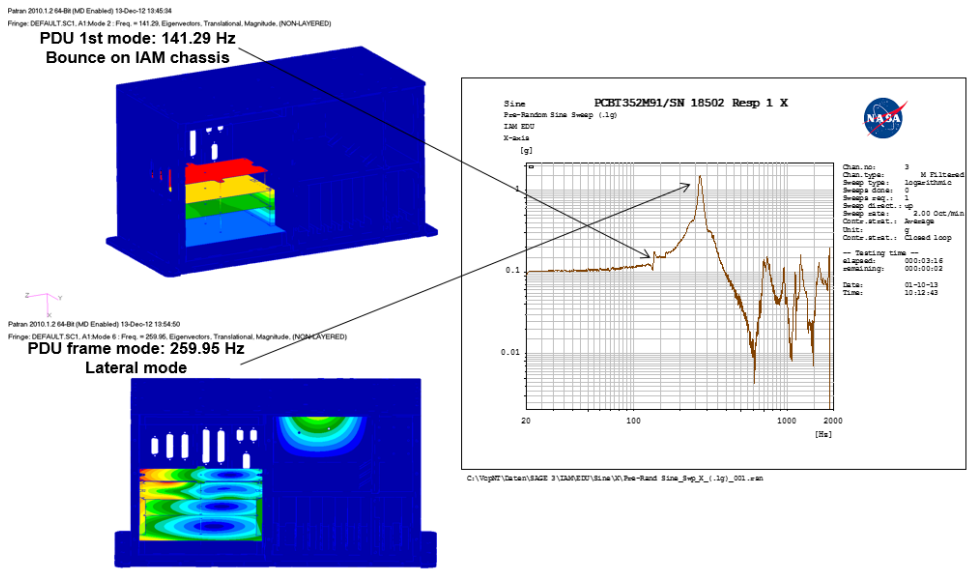

Figure 6: Modal Analysis Result and Test Data for IAM PDU

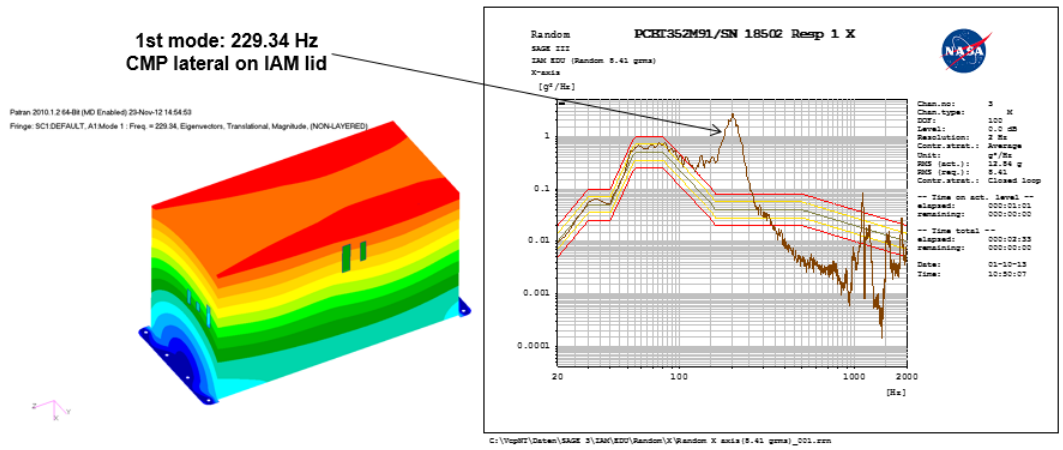

Figure 7: Modal Analysis Result and Test Data for IAM Chassis

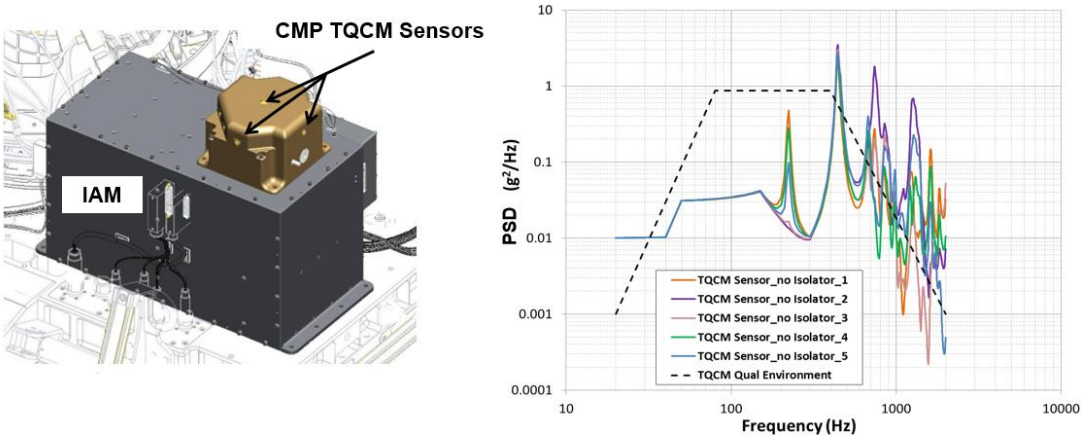

Figure 8: CMP High-Frequency Responses at TQCM Sensor Locations from Analysis

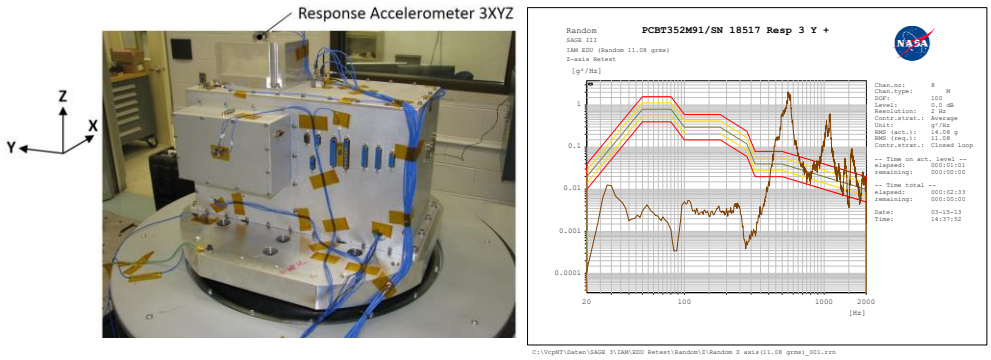

Figure 9: CMP High-Frequency Response in Y-Axis Due to IAM Interface Z-Axis Random Test Level

4. Three-Dimensional Vibration Isolator and FE Model with Isolators

The selected Enidine CR6-100 WRI consists of a top mounting bar, a bottom mounting bar, and a stainless steel wire cable as shown in Figure 10. It weighs a quarter pound and has a size of 2 inches wide by 2 inches long by 2 inches high configuration. Since no vendor data was available for tension loads in the vertical direction, four CR6-100 WRI test articles were used in a stiffness test carried out at NASA Langley material lab. It is seen from test data shown in Figure 11 that for the CR6-100 WRI, the tension stiffness is different with the compression stiffness in all three directions, particularly in vertical direction where the tension stiffness is much larger than the compression stiffness in the displacement area above 0.1 inch. However, the compression stiffness is a little bit larger than the tension stiffness in the shear 1 and 2 directions at displacements greater than 0.6 inch. While these stiffness coefficients are nonlinear the WRI normally operates at small displacements. Two CR6-100 WRI test articles were used in a failure test carried out at NASA Langley material lab. It is seen from test data shown in Figure 12 that the CR6-100 WRI can withstand tremendous load up to 4000 lbf in the vertical and shear directions. The failure mode is the wire cable pulling out of the mounting bar with partial connection capacity without causing catastrophic connection failure between the CMP and IAM. The CR6-100 WRI stiffness coefficients and the failure modes in all directions captured in tests are published here for the first time.

The WRIs were incorporated into the FE model by using BUSH elements after their stiffness coefficients had been obtained, as shown in Figure 10.

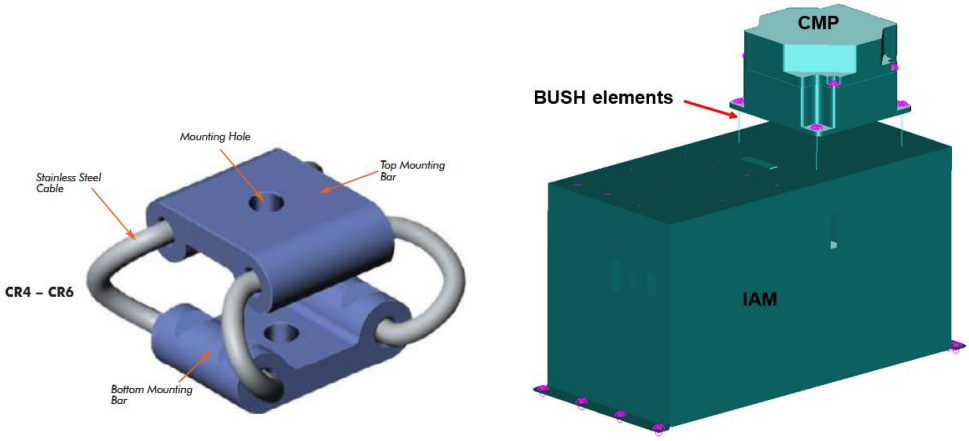

Figure 10: Selected CR6-100 Isolator and FE Model (not showing mesh) with Isolators

Based on the mass W of CMP (about 6.5 lbs.) and the stiffness k of the selected CR6-100 isolator (about 180 lbs./in in the vertical direction), the isolated CMP natural frequency is calculated by the equation (2):

$$\frac{1}{2\pi}\sqrt{\frac{k\times g}{W}}=\frac{1}{2\times 3.14}\sqrt{\frac{(4\times 180.)\times 386.}{6.5}}=33.\ \text{Hz} \quad (2)$$

This response can be observed from the simulation result shown in Figure 13 (the first peak in the response curves). The result was used to verify the FE model and the random analysis.

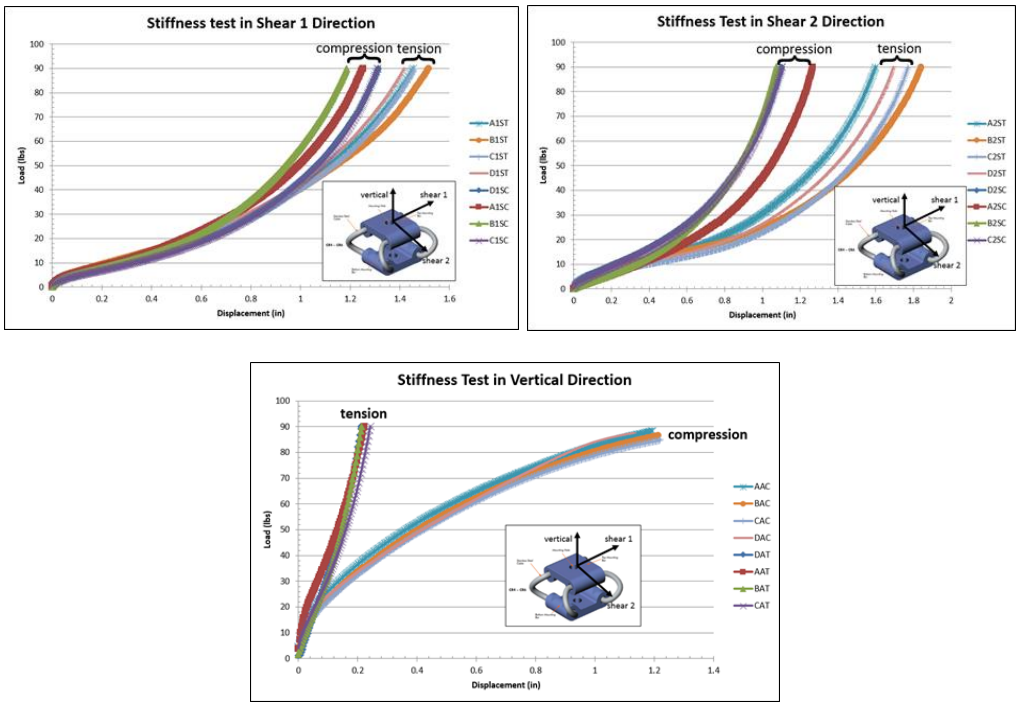

Figure 11: Selected CR6-100 Isolator Stiffness Test

Figure 12: Selected CR6-100 WRI Failure Test

5. Analysis and Test for Isolator Verification

By using the FE model with the isolators, random analyses due to the SpaceX launch random loads were conducted and it was verified that all high-frequency responses on the CMP interface are reduced by several orders of magnitude over a wide frequency range compared to those without the isolators. For instance, as shown in Figure 13, the responses in the z direction at 4 sensor locations on the CMP interface due to the SpaceX launch random load in the z direction are reduced by

several orders of magnitude over the wide frequency range compared to that without the isolators in the red curve. From analysis results, it was noticed that in some cases the responses in a low frequency range from 20 to 100 Hz with the isolators are higher than those without the isolators as shown in Figure 13. Considering that the first natural frequency of the CMP alone is high (above 700 Hz) and the TQCM sensor natural frequency is even higher (at least 3 MHz), we treated the CMP and the sensors as rigid bodies only with limited g values associated with the responses that will not cause any damage to the sensors and the CMP structure. In addition, test data shown in Figure 14 indicates that these responses at the low frequency range are reduced without the peaks due to the high damping in reality (2% modal damping was used in analysis). Test data in the upright setup shown in Figure 14 shows that all high-frequency responses on the CMP interface are reduced by several orders of magnitude over the wide frequency range as predicted in analysis. For instance, as shown in Figure 14, the response in the z direction at a sensor location on the top panel of the CMP due to the SpaceX launch random load in the z direction is reduced by several orders of magnitude over the wide frequency range.

Since the SAGE III payloads will be mounted upside-down during the SpaceX launch, the highest random loads are applied and the isolators are under tension, analysis and test were conducted to verify the isolators showing similar effective suppression behaviour on the high-frequency responses in an inverted configuration. For instance, as shown in Figure 15, test data from the inverted test setup indicates that the response in the z direction at a sensor location on the top panel of the CMP due to the SpaceX launch random load in the z direction is reduced by several orders of magnitude over the wide frequency range.

After the isolators had been verified by analysis and test, they were incorporated into an updated SAGE III on ISS configuration shown in Figure 16.

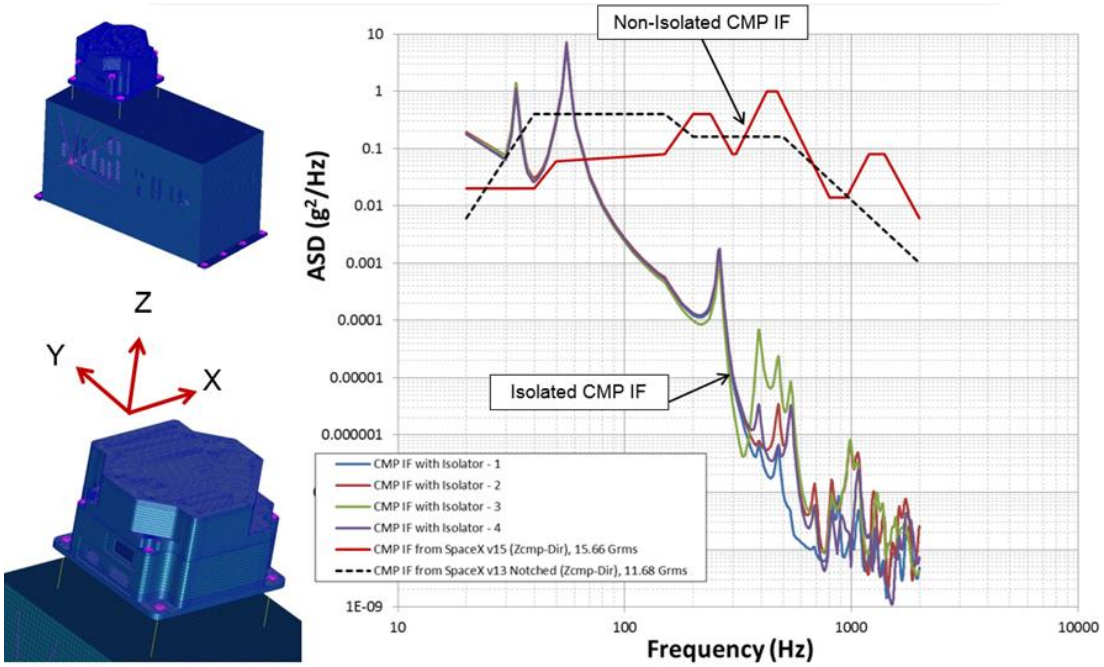

Figure 13: Random Analysis for Isolator Verification

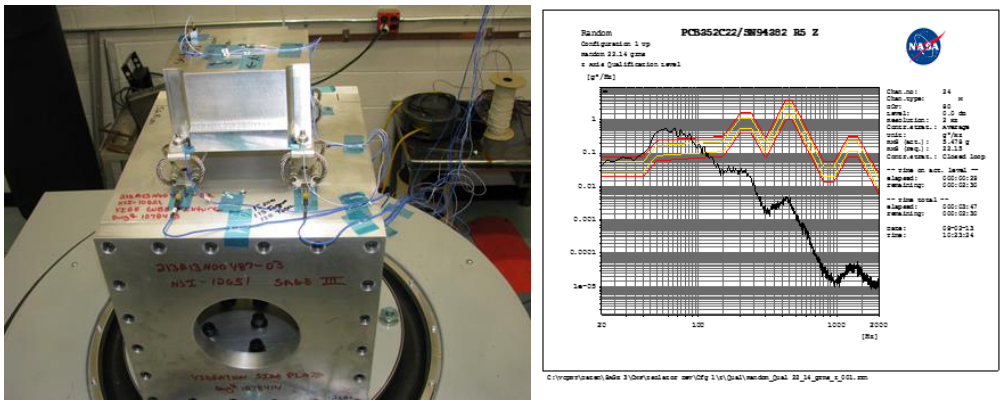

Figure 14: Upright Test Setup and Isolator Verification Test

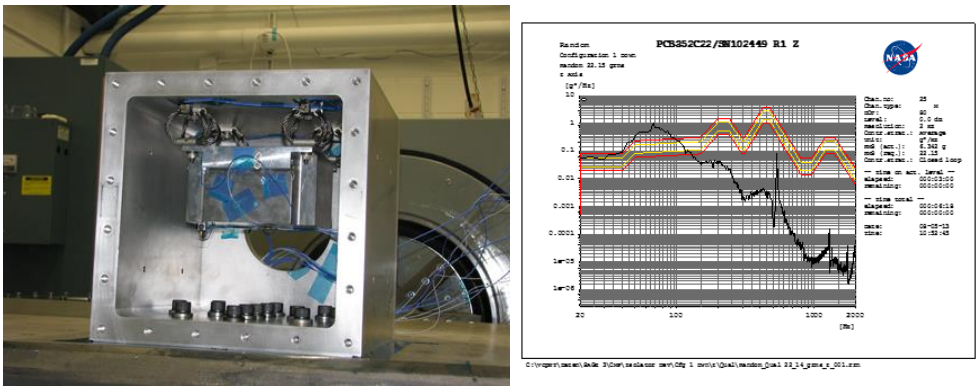

Figure 15: Inverted Test Setup and Isolator Verification Test

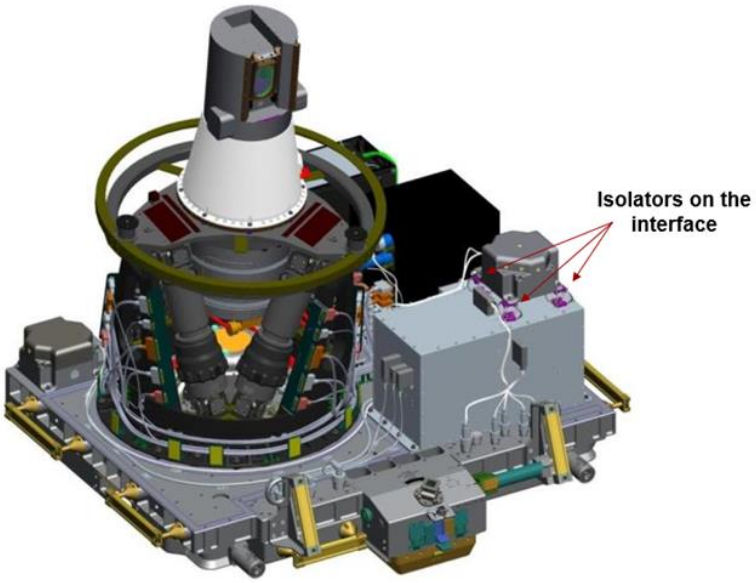

Figure 16: Updated SAGE III on ISS Configuration

6. Concluding Remarks

When the SAGE III on ISS CMP was designed to be mounted on the top panel of the IAM, the configuration caused a structure coupling causing the CMP to experience high-frequency responses, which might damage the internal electronic cards and the TQCM sensors. The CR6-100 WRIs were proposed and selected to be inserted at the interface between the CMP and the IAM in order to attenuate the high-frequency responses without causing any major changes to the existing system. Due to complexity of the IAM, two FE models with majority of shell

elements or solid elements were constructed respectively to simulate the IAM for required structural analyses. It is recommended for a complex structure such as the IAM to build different detail-level FE models to capture different characteristics of the system. For a simple structure such as the CMP, a detailed FE model was constructed at first to satisfy the analysis needs. From analysis simulation results and test data, it was shown that by using the 3D wire rope isolators the CMP high-frequency responses have been reduced by several orders of magnitude over the critical frequency range (from 700 Hz to 2000 Hz) under the upright and inverted CMP mounting configurations. The TQCM sensor responses were well below their qualification environments when the WRIs were used to isolate the CMP.

7. References

1. Bronowicki, Alien, “Vibration Isolator for Large Space Telescopes,” Journal of Spacecraft and Rocket, Vol. 43, No. 1, January–February 2006.

2. Rahman, Zahidul; Spanos, John, “Six axis vibration isolation, suppression and steering system for space applications,” AIAA Dynamics Specialists Conference, Salt Lake City, UT, Apr. 18, 19, 1996.

3. Murphey, Thomas; Botke, Matthew; Blankinship, Ross; Hague, Tyler, “An Articulated Motion and Vibration Isolator for Spacecraft,” 44th AIAA/ASME/ASCE/AHS Structures, Structural Dynamics, and Materials Conference, 7-10 April 2003, Norfolk, Virginia.

4. Miao, Xuhong; Zheng, Gangtie, “Analytical Study of Whole Flexible Spacecraft Vibration Isolation”, 49th AIAA/ASME/ASCE/AHS/ASC Structures, Structural Dynamics, and Materials Conference, 7 - 10 April 2008, Schaumburg, IL.

5. Camelo, Vanessa; Bronowicki, Allen; Simonian, Stepan; Hejal, Reem; Brennan, Sarah, “Damping and Isolation Concepts for Vibration Suppression and Pointing Performance,” 50th AIAA/ASME/ASCE/AHS/ASC Structures, Structural Dynamics, and Materials Conference, 4 - 7 May 2009, Palm Springs, California.

6. Gandhi, Farhan; Anusonti-Inthra, Phuriwat, “Helicopter Vibration Reduction Using Discrete Controllable-Stiffness Devices at the Rotor Hub,” 42nd AIAA/ASME/ASCBAHS/ASC Structures,

Structural Dynamics, and Materials Conference and Exhibit, 16-19 April 2001, Seattle, WA.

7. Swanson, Douglas; Miller, Lane; Norris, Mark, "Multidimensional Mount Effectiveness for Vibration Isolation," Journal of Aircraft, Vol. 31, No. 1, Jan.-Feb. 1994.

8. Belvin, Keith; Sparks, Dean, "On the Isolation of Science Payloads from Spacecraft Vibrations," AIAA-95-26617.

9. Johnson, Conor; Wilke, Pau, "The Whole-Spacecraft Vibration Isolation System- Its Time Has Come," AIAA Space Technology Conference & Exposition, 23-30 Sept. 1999 Albuquerque, NM.